HIGH DYNAMIC RANGE PHOTOGRAPHY WITHOUT A TRIPOD: A LINEAR FORMULATION FOR IMAGE FUSION

This paper presents a new multi-image registration methodology able to align a set of hand-held bracketed shots. The procedure is a two-step algorithm where (i) corresponding multi-image points are automatically extracted from the bracketed image sequence and (ii) a Least Squares adjustment recovers transformation parameters. This methods allows photographers to acquire several bracketed pictures with their hand-held digital cameras. Then, images can be processed with High Dynamic Range algorithms in order to combine multiple Low Dynamic Range pictures into a single mosaic with a superior radiometric quality. Simulated and real examples are illustrated to prove the effectiveness of the developed affine-based procedure.

1   Introduction

Professional and consumer-grade digital cameras have had an incredible impact on people. Digital photography changed the way people capture, modify, and share images. Almost everyone has a digital camera today, as it is one of the easiest tools to capture, store and remember our special memories.

In recent years, the rapid development of digital camera technology has provided sensors with high radiometric and geometric resolutions and good storage capacity. The global digital camera shipment is impressive: 130 million units in 2009, 141 million units in 2010, and 145 million units in 2011. However, the year 2012 marks a global decline in camera sales, that continued to diminish in 2013. Indeed, with the rapid diffusion of the use of smartphones and tablets, casual snapshooters tend to capture images with portable devices where images can be easily modified, enhanced, and shared in the Cloud. Several websites offer the possibility to visualize collections of images and videos of any size (e.g. Facebook, Flickr, Google, …).

If photography has been a chemical process for over 150 years, nowadays films, chemicals or dark rooms are things of the past, exception made for some professional camera models still used by expert photographers.

The geometric process for the creation of a digital photograph requires the alignment of the (i) perspective center of the image, the (ii) object point and its (iii) projection on the image plane (pinhole camera model, Hartley, 1994). Most digital cameras follow this condition (*collinearity principle*) and are termed *central perspective* cameras (Stamatopoulos and Fraser, 2013). It is important to mention that other camera models are available on the commercial market. For instance, a camera with a fisheye lens does not follow the pinhole camera, whereas push-broom sensors are often employed in the case of aerial and satellite images for remote sensing purposes. In some cases, special line-based panoramic cameras are used in terrestrial applications for 3D modeling. This kind of images are not taken into consideration in this work.

As most low cost and professional cameras capture pinhole images, this paper focuses on this particular kind of data, notwithstanding the collinearity principle is satisfied in the case of an ideal cameras. In fact, an image taken with a real camera-lens system has a residual geometric distortion. The error for image distortion can be reduced in the case of long focal lenses (telephoto lenses), although a small residual distortion effect remains visible. A *calibrated camera* (Fraser, 2013) can be intended as a sensor able to produce distortion-free images with a geometric model for data correction. This means that distortion coefficients are known from a preliminary calibration project (Cronk et al., 2006) and a new distortion-free image can be created by resampling the original image. Some software have a database of correction coefficients and can remove image distortion beforehand (e.g. PTlens).

One of the most remarkable advantages of digital images is the opportunity to run processing algorithms able to modify, enhance, and register multiple shots. Many software (for both personal computers or mobile phones and tablets) are available on the commercial market. In this paper the particular case of *High Dynamic Range* (HDR) photography is discussed (Yu et al., 2011).

High Dynamic Range photography captures the complete dynamic range of light in real scenes in order to increase the radiometric quality of the images. Modern charge-coupled device (CCD) or complementary metal oxide semiconductor (CMOS) sensors have spatial resolutions superior to 20-30 megapixels. When a customer wants to buy a digital camera, it is normal for non-expert photographer to be attracted by the number of pixels (i.e. the geometric resolution). On the other hand, one of the most important factors is the metric pixel size (small pixels give noisy images) along with the radiometric resolution.

The discretization carried out by digital cameras involves (i) the spatial domain (the grid behind pixel distribution) and (ii) the radiometric resolution connected to the image depth (number of bits per pixel, i.e., grey values - gv). A color image is a discrete function $gv = gv(x, y)$ where light intensity information is associated to pixel location (x, y). A standard digital camera has three channels (r, g, b) that correspond to red, green and blue components. A filter on the sensor (Bayer filter mosaic) allows a pixel to capture a single light component, then an interpolation is carried out to recover lost or missing information. Other cameras are instead based on Foveon technology and can directly measure the different components by means of a layered sensor structure (three vertically stacked photodiodes).

A good digital camera should capture a sufficient dynamic range (the ratio between the maximum and minimum pixel values) in order to simulate human vision. The human visual system is very sensitive to wavelengths in the visible spectrum (from approximately 400 to 800 nm) and can deal with strong changes in brightness in order to preserve the original color of the scene. The human eye has optimal adaptation mechanisms that allow one to see real scenes with dynamic ranges exceeding five orders of magnitude. On the other hand, a common digital camera acquires only Low Dynamic Range (LDR) images where the full dynamic range of light cannot be correctly reconstructed.

This sensor's limitation can be removed by means of a set of multiple LDR images acquired with different exposures (bracketed images). LDR pictures can be merged after a preliminary geometric alignment. First, the sensor's spectral response function must be determined. Then, images acquired at different exposures can be transformed into a single high dynamic radiance map (Ikebe, 2013).

There exist several methods to overcome this problem. However, one of the most significant contribution for HDR photography is described in Debevec and Malik (1997, 2008), where a reliable solution was illustrated. It is based on the hypothesis that the response function is invertible and smooth. The method is very attractive and several packages for HDR composition are today available (e.g. Hydra, Photomatix, Photo Merge, Photoshop). Moreover, several apps can be downloaded from the Internet in order to create HDR mosaics with portable devices. Their use is quite simple and almost fully automated (Tiant et al, 2012).

For these reasons, HDR imagery is very attractive not only for expert photographers (or expert operators involved in the fields where images are used for advanced purposes, for instance photogrammetry, virtual reality, computer vision, etc., see Barazzetti et al., 2011 and Cai et al., 2013), but also for beginners who want to store their special memories with an interesting photographic technique able to increase the radiometric resolution of the camera.

A tripod is a standard solution to acquire aligned images for High Dynamic Range photography. On the other hand, the possibility to use a hand-held digital camera is surely more practical for photographers and casual snapshooters, especially if mobile devices are employed. In the case of hand-held images, one of the problem is the lack of pixel correspondence between two (or more) bracketed pictures. Indeed, HDR algorithms rely on pixel correspondences and therefore the camera should be installed on a tripod to ensure that all images align correctly. Moreover, the scene should be as static as possible in order to avoid artifacts.

In this paper a registration algorithm that recovers the alignment of several bracketed hand-held images by using a global adjustment is presented. Registration parameters are estimated from a set of image correspondences automatically extracted from the images. Then, an affine-based multi-view Least Squares adjustment includes all the images into a global registration where residual misalignments are removed. Finally, the set of bracketed pictures will be resampled in order to overlap with sub-pixel precision.

2 Matching bracketed images

2.1 Splitting a block into pairs

The procedure for image alignment needs a set of corresponding points to estimate the transformation parameters of the images. The automated image matching algorithm can be considered as a progressive process (Fig. 1) where multiple bracketed pictures are analyzed independently, then image points are reordered (i) to find corresponding points on multiple images and (ii) to run the affine-based global adjustment.
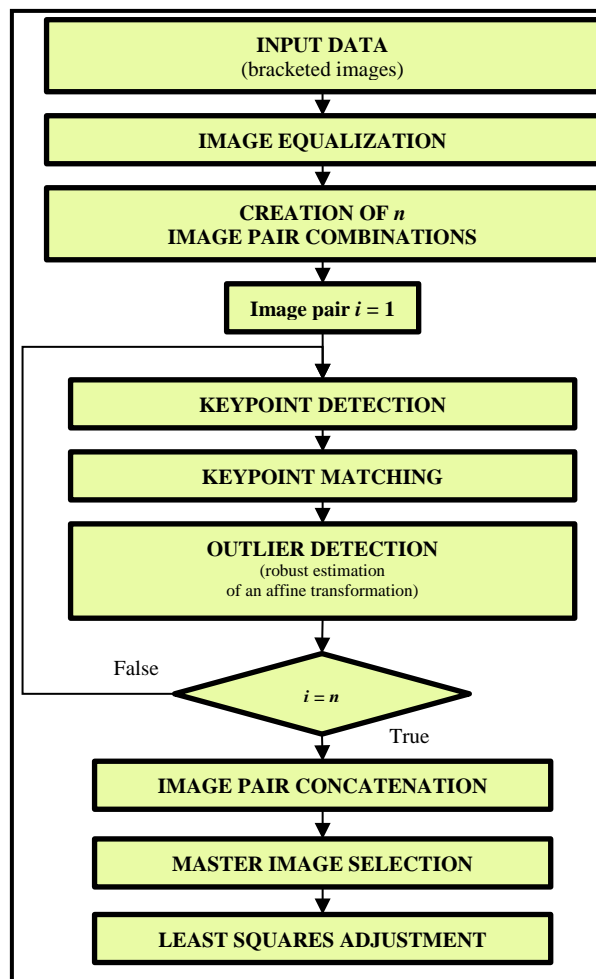

Figure 1 The flowchart of the implemented algorithm for image alignment.

The core of global processing is based on a preliminary subdivision of the original bracketed images into different pairs. In the case of w LDR images, a total number of $w(w-1)/2$ independent image combinations is used for further matching purposes: data processing is also parallelizable because image pair remain independent in the preliminary matching step.

2.2 Pairwise matching

The developed methodology starts extracting features with the SIFT (Scale Invariant Feature Transform) and SURF (Speeded-Up Robust Features) operators (Lowe, 2004; Bay et al., 2008). The choice of the operator is performed by the user. Both operators are very robust against outliers (robustness is needed for automated matching where a significant percentage of outliers can be found). Moreover, both operators are translation- rotation, and scale- invariant because a movement of the perspective center is expected for hand-held photos.

The SIFT and SURF operators are very used in applications carried out with terrestrial (close-range) images like photogrammetry and computer vision, where sub-pixel precision is needed in the image orientation step (bundle adjustment). The technical literature reports some scientific contributions where both methods where extended to handle specific situations. In most cases some improvements were performed to increase their performances (Cai et al, 2014; Lee et al., 2013).

The scale invariant feature transform (SIFT) is a standard algorithm in computer vision applications (such as object recognition, Structure from Motion, and data registration) because it provides highly distinctive features that are invariant to image scaling and rotation. The functioning of this operator can be split into four steps: scale-space extreme detection, keypoint localisation, orientation assignment, and keypoint descriptor creation. The implementation of the SURF operator is instead derived from the original code available at http://www.vision.ee.ethz.ch/~surf/, and the descriptor is a vector made up of 128 elements. The method uses a Hessian matrix-based measure for the detector and the distribution of the first-order Haar wavelet responses for the descriptor.

Corresponding features can be found by comparing the descriptors with the Euclidean distance, without any preliminary information (Barazzetti et al., 2009). In addition, the ratio test with threshold 0.75 is used to obtain more distinctive matches. When the operator retrieves a sufficient number of image correspondences, some mismatches are often still present. The procedure uses the robust estimation of an affine transformation between the corresponding features to reject these outliers.

Obviously, this assumes that the geometric model that connects the bracketed images is an affinity (more details about the proposed mathematical model are given in section 3). Given a set of corresponding image points $\boldsymbol{x}_k = (x_k, y_k, 1)^T \leftrightarrow \boldsymbol{x}_k' = (x_k', y_k', 1)^T$ between two images (written in homogeneous coordinates), the condition:

$$x'_k = \begin{bmatrix} x'_k \\ y'_k \\ 1 \end{bmatrix} = \begin{bmatrix} a & b & c \\ d & e & f \\ 0 & 0 & 1 \end{bmatrix} \begin{bmatrix} x_k \\ y_k \\ 1 \end{bmatrix} = \mathbf{H}x_k \qquad (1)$$

must be checked. The estimation of $\mathbf{H}$ needs to be coupled with robust techniques as they allow the detection of possible outliers in the observations. The proposed methods is based on the analysis of several sets of image coordinates randomly extracted from the whole dataset. In this procedure the high breakdown point estimator RANSAC is included. Outliers can be identified and removed with an iterative process where several $\mathbf{H}$ matrices are estimated. A minimum number of trials m is given by:

$$m = \frac{log(1-P)}{log\left(1-(1-e)\right)^s} \qquad (2)$$

where P is the probability from a given size of sample s, with a percentage of outliers e. The goal is the extraction of a good subset of m corresponding points $[x_k \leftrightarrow x_k']$ where outliers are rejected and the transfer error:

$$d_r^2 = d(x, H^{-1}x')^2 + d(x', Hx)^2 \qquad (3)$$

is minimum. The random selection of points is carried out by considering their distribution in the images because the computed affinity is extended to the whole image.

Once a good set of features without outliers is extracted, $\mathbf{H}$ can be computed by using the correct matches and standard Least Squares techniques. This last estimate is carried out to check point precision in terms of pixel coordinates.

2.3 Matching multiple Low Dynamic Range images

As mentioned, the main advantage of the proposed methodology is the global registration of all the bracketed images. The procedure for single pair matching previously described is therefore repeated for all image pairs in order to determine a set of pairwise corresponding features. Obviously, the algorithm could remove some image pair combinations from further data processing when points are missing or when only a few points are available (an empirical threshold of at least 40 corresponding points was set).

On the other hand, it is possible that some pairwise matches are simultaneously "visible" in several images. Data (image coordinates in this case) need to be clustered into a regular structure (track) in order to identify points visible in as many images as possible. The problem becomes similar to the extraction of tie points from blocks of images used for 3D modeling (Brumana, 1990; Oreni et al., 2012), where points with a higher geometric multiplicity are sought to improve network geometry.

The same concept is here replicated by considering the numerical value of image coordinates. A characteristic of the proposed detectors is their good repeatability, i.e. the capability of finding the same point under different illumination conditions (bracketed images). A progressive check of the extracted pixel coordinates provides a regular structure of image coordinates, similar to the input of a standard bundle block adjustment (Liu et al., 2012).

3   Linear multi-image alignment

The mathematical model used to recover a missing alignment of LDR images is based on a simultaneous multi-affine transformation. An affine transformation (or affinity) is a linear transformation which preserves points, straight lines, and planes. Parallel lines remain parallel after an affine transformation, whereas angles between lines or distances between points are not necessary preserved, though it does preserve ratios of distances between points lying on a straight line.

The implemented algorithm assumes an image as reference (called 'master') to overcome the "datum problem", i.e. the rank deficiency for the lack of a stable reference system. The images are ordered according to the exposure value (EV), then the central one becomes the reference. The remaining images ('slaves') are mapped on the master reference system.

As the method aims at registering multiple images by means of a global adjustment, corresponding points are needed not only for 'master-to-slave' image combinations, but also for all 'slave-to-slave' image pairs.

A geometric registration technique that simultaneously estimates all parameters was developed. The proposed algorithm replicates the effect of bundle adjustment (Ji et al., 2012), making the estimation phase more accurate and reliable.

As mentioned, the geometric model used in this study is an affinity between the image point coordinates on the pair of images (x, y and x', y'):

$$x'_{iM} = \underline{a}_j x_{ij} + \underline{b}_j y_{ij} + c_j \;\; ; \;\; y'_{iM} = \underline{d}_j x_{ij} + e_j y_{ij} + f_j \tag{4}$$

where i is point index and j image index (the underlined quantities are the unknowns). These equations (4) describe the transformation between a 'master-to-slave' pair, whereas equations (5):

$$\underline{a}_j x_{ij} + \underline{b}_j y_{ij} + c_j - \underline{x}'_{ij} = 0 \;\; ; \;\; \underline{d}_j x_{ij} + \underline{e}_j y_{ij} + f_j - \underline{y}'_{ij} = 0 \tag{5}$$

are needed for a point matched on slave-to-slave combinations.

This mathematical model assumes that each image j will be resampled by using an affine transformation in order to obtain pixel correspondence with the master image (marked with index 'M').

Equations (4) (for standard 'master-to-slave' matching) are not analyzed independently but they are included in the same system (the algorithm checks if different pairs share the same points). Points on the master image are intended as fixed coordinates and are used to remove the rank deficiency (6 parameters) of the normal matrix of Least Squares.

Equations (5) are used to improve the connection between the images and to strengthen block geometry. In addition, they limit the number of 'master-to-slave' point (like in a photogrammetric bundle adjustment where the number of ground control points can be reduced thanks to a set of additional tie points) and provide the registration parameters of the images without a direct visibility with the master. The unknown pixel coordinates of these points correspond to features matched in two or more slaves and then reprojected on the master.

As points are extracted with the same operator (SIFT or SURF) we assume that they have the same pixel precision. This mathematical formulation fixes the points of the master image and define a stable reference system. The solution here proposed could be intended as an independent model adjustment where the datum is fixed by the points extracted from the master image.

Given p image points (after data reordering, as explained in the following section), $2p$ equations can be written. The redundancy depends on the number of images (w), i.e., six geometric parameter per every image, the coordinates of 'slave-to-slave' matches reprojected onto the master (m) and the number of 2D points (u) used as reference. The redundancy (r) of this system becomes:

$$r = 2p - 6(w - 1) - 2m + 2u \qquad (6)$$

The linear system of normal equations has the form:

$$Nx = \begin{bmatrix} A_1 & \overline{N} \\ \overline{N}^T & A_2 \end{bmatrix} \begin{pmatrix} x_1 \\ x_2 \end{pmatrix} = \begin{pmatrix} n_1 \\ 0 \end{pmatrix} = b \qquad (7)$$

where x_1 contains the unknown transformation parameters ($a_j, b_j, c_j, d_j, g_j, f_j$) of image j and x_2 the image coordinates of slave-to-slave point projected on the master image. N has a particular banded form (Fig. 2), where:

- A_1 is a hyper-diagonal matrix with sub matrices 6×6 corresponding to individual images;
- A_2 is a $2m \times 2m$ diagonal matrix.

Finally, the solution and its precision (variance-covariance matrix) are obtained with standard Least Squares techniques (Gauss-Elimination Method in this case).
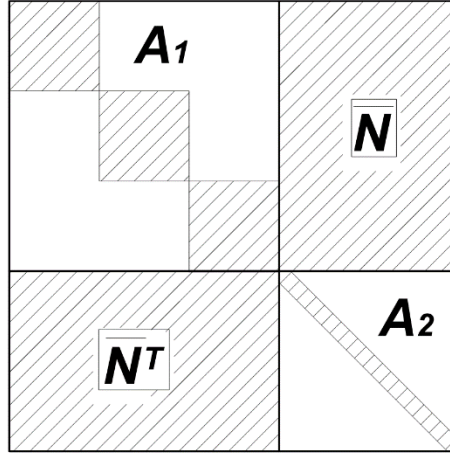
Figure 2 The normal matrix of LS adjustment

4 Case studies

4.1 How to bracket photos

Images can be acquired by taking some underexposed brackets, the central bracket, and the overexposed ones. This is usually carried out by setting the camera in manual or aperture priority mode with the right F-number dialed in, a low ISO, without flash, and anti-shake turned off. This procedure (coined *bracketing*) can be defined as the acquisition of the same photograph several times using different settings for different exposures. Most professional cameras have a proper Automatic Exposure Bracketing (AEB) function where three, five, seven, nine (or more) images will be acquired with just one click of the shutter, each in different exposures. The result will be a set of bright pictures (in a progressive order), one just right and the remaining ones are progressively dark.

4.2 Geometric alignment of hand-held pictures

A sequence of 5 bracketed pictures (-2 EV, -1 EV, 0 EV, +1 EV, +2 EV) was acquired inside a basilica (Fig. 3) with strong backlights (rose window by day). The camera used is a Nikon D700 (full-frame camera, 4256×2832 pixels, pixel size 0.0084 mm, automatic bracketing function) equipped with a 20 mm lens. It is important to notice that the short focal length mounted on the full-frame sensor (36 mm × 24 mm) gave very strong image distortions, making the matching/registration phase more complicated. For this reason, this is a good benchmarking dataset for the proposed algorithm.

Figure 3 The sequence of bracketed pictures.

Matching was run by using the SURF operator obtaining a total number of 16,607 image points after the pairwise matching phase. Fig. 4 shows the matching result for a generic pair.
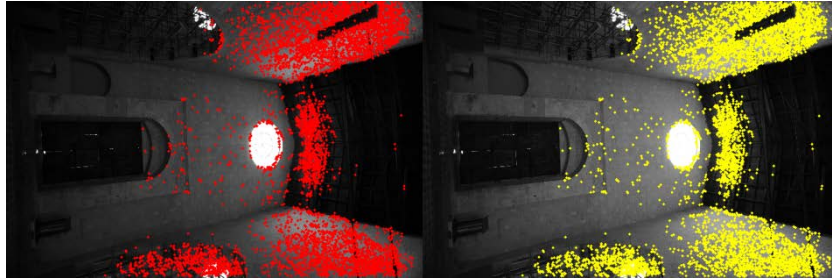

Figure 4 Automated matching result for a generic image pair.

The normal matrix of the LS problem is shown in Fig. 5, where a detail highlight the banded form of the part corresponding to transformation parameters.
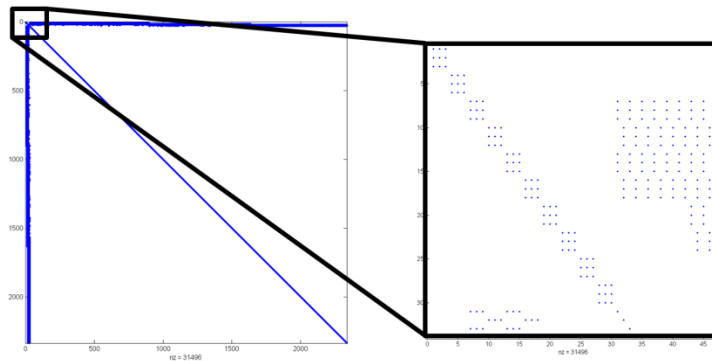

Figure 5 The normal matrix (left) and a detail of the part corresponding to affine parameters (right).

The Least Squares problem includes 33,214 equations and 2,336 unknowns (redundancy is 30,878). The final sigma-naught was ±0.434 pix (a priori sigma-naught was set to 1), i.e. sub-pixel precision. The final HDR image was generated after resampling the single images according to the estimated multi-affine parameters (Fig. 6). Global data processing (alignment and HDR image

generation) took less than 3 minutes with an Intel® Core(TM) i7-2760QM, CPU 2.4 GHz, 16 GB RAM.

Figure 6 The final HDR image and a detail showing the correct registration (misalignments are not visible).

4.3 Example with open data

The algorithm was then tested with a sequence of images downloaded from the Internet. The scene is the Jefferson National Expansion Memorial and the Gateway Arch and Old Courthouse, in St. Louis, MO, USA. Images were taken at night as part of a set of different exposures. The photographer is Kevin McCoy and files are licensed under the Creative Commons Attribution-Share Alike 3.0 Unported license. The camera used (data were recovered from EXIF information) is a Canon PowerShot S3 IS (focal length is 7 mm). Shots were acquired with EV -4.72, -1.82, +1.51, and +4.09, respectively (Fig. 7).

Figure 7 The images of the Jefferson National Expansion Memorial downloaded from the Internet.

Figure 8 The HDR image created from 4 LDR pictures downloaded from the Internet.

One of the most important points concerns the possible use of a stable set up. It is unknown the procedure for data acquisition and for this reason the algorithm for image registration was run beforehand.

The pairwise matching phase was able to find corresponding matches for the image combinations (1,2), (1,3) and (3,4). This means that the last image is not robustly connected to the other others, although the combined adjustment is still feasible because all images have common points and form a block. The balance equations - unknowns was 2,338 vs 270 (redundancy is 2,068) and the estimated sigma-naught was ±0.426 pixels, confirming sub-pixel precision also for this second example.

The variance-covariance matrix gave the precision of the estimated parameters. It is interesting to check the value of parameters (c_j, f_j) because they represent translations and their numerical values (in pixels) can give information about the quality of the solution. For a generic image j, the precision of the translation parameters is the same in both x and y directions ($\sigma_{cj} = \sigma_{fj}$).

Images "2" and "3" (that are well connected with the master – image "1" in this case) have a precision equal to $\sigma_{c2} = \sigma_{f2} = \pm0.21$ pix, and $\sigma_{c3} = \sigma_{f3} = \pm0.18$ pix. The last image (connected with image "3" only) has a worse precision $\sigma_{c4} = \sigma_{f4} = \pm0.41$ pix. On the other hand, the considered images (even image "4") were registered with sub-pixel precision, that is more than sufficient to remove the initial misalignment. The final HDR image after image registration is shown in Fig. 8.

5 Conclusion

This paper presented a new methodology able to align a set of bracketed images acquired with a hand-held digital camera, where several images are automatically resampled in order to obtain pixel correspondence for HDR image generation.

The implemented solution uses SIFT or SURF features in order to extract a set of multi-image points. Robust estimators remove wrong matches and standard Least Squares techniques provide transformation parameters and allow the operator to check the quality of the solution. The implemented affine-based adjustment derives the unknown parameters with a reliable processing workflow that simultaneously exploits not only independent image combinations, but also the entire dataset along with multiple image connections.

The final result is in a new set of LDR images that overlap with sub-pixel precision. These images are suitable for HDR photography in the case of hand-held sensors, such as low cost and professional cameras (without tripods) or mobile phones and tablets.

The method was tested on several real cases and two experiences were illustrated in this work. The obtained precision of the registration phase was more than sufficient to obtain a HDR mosaic of the scene.

References

Bay, H., Ess, A., Tuytelaars, T. & Van Gool, L. 2008, "Speeded-Up Robust Features (SURF)", *Computer Vision and Image Understanding,* vol. 110, no. 3, pp. 346-359.

Barazzetti, L., Remondino, F. & Scaioni, M. 2009, "Combined use of photogrammetric and computer vision techniques for fully automated and accurate 3D modeling of terrestrial objects", *Proceedings of SPIE - The International Society for Optical Engineering.*

Barazzetti, L., Forlani, G., Remondino, F., Roncella, R. & Scaioni, M. 2011, "Experiences and achievements in automated image sequence orientation for close-range photogrammetric projects", *Proceedings of SPIE - The International Society for Optical Engineering.*

Brumana, R. 1990, "Sant'Ambrogio's Basilica in Milan. A study on photogrammetric surveys in the S. Vittore in Ciel d'Oro's dome", *Proceedings of SPIE - The International Society for Optical Engineering,* pp. 908.

Cai, H. 2013, "High dynamic range photogrammetry for light and geometry measurement", *AEI 2013: Building Solutions for Architectural Engineering - Proceedings of the 2013 Architectural Engineering National Conference*, pp. 544.

Cai, S., Liu, L., Yin, S., Zhou, R., Zhang, W. & Wei, S. 2014, "Optimization of speeded-up robust feature algorithm for hardware implementation", *Science China Information Sciences,* , pp. 1-15.

Cronk, S., Fraser, C. & Hanley, H. 2006, "Automated metric calibration of colour digital cameras", *Photogrammetric Record,* vol. 21, no. 116, pp. 355-372.

Debevec, P.E. & Malik, J. 1997, "Recovering high dynamic range radiance maps from photographs", *Proceedings of the ACM SIGGRAPH Conference on Computer Graphics*, pp. 369.

Debevec, P.E. & Malik, J. 2008, "Recovering high dynamic range radiance maps from photographs", *ACM SIGGRAPH 2008 Classes*, pp. 31.

Fraser, C.S. 2013, "Automatic camera calibration in close range photogrammetry", *Photogrammetric Engineering and Remote Sensing,* vol. 79, no. 4, pp. 381-388.

Hartley, R.I. 1994, "Projective reconstruction and invariants from multiple images", *IEEE Transactions on Pattern Analysis and Machine Intelligence,* vol. 16, no. 10, pp. 1036-1041.

Ikebe, M. 2013, "High dynamic range imaging and local adaptive tone mapping", *Proceedings of SPIE - The International Society for Optical Engineering*.

Ji, S., Shi, Y. & Shi, Z. 2012, "Bundle adjustment with vehicle-based panoramic imagery", *Proceedings of the 2nd International Workshop on Earth Observation and Remote Sensing Applications, EORSA 2012*, pp. 106.

Lee, M.H. & Park, I.K. 2013, "Robust feature description and matching using local graph", *2013 Asia-Pacific Signal and Information Processing Association Annual Summit and Conference, APSIPA 2013*.

Liu, X., Sun, F.-. & Hu, Z.-. 2012, "Distributed bundle adjustment in 3D scene reconstruction with massive points", *Zidonghua Xuebao/Acta Automatica Sinica*, vol. 38, no. 9, pp. 1428-1438.

Lowe, D.G. 2004, "Distinctive image features from scale-invariant keypoints", *International Journal of Computer Vision,* vol. 60, no. 2, pp. 91-110.

Oreni, D., Brumana, R. & Cuca, B. 2012, "Towards a methodology for 3D content models: The reconstruction of ancient vaults for maintenance and structural behaviour in the logic of BIM management", *Proceedings of the 2012 18th International Conference on Virtual Systems and Multimedia, VSMM 2012: Virtual Systems in the Information Society*, pp. 475.

Stamatopoulos, C. & Fraser, C.S. 2013, "Target-free automated image orientation and camera calibration in close-range photogrammetry", *American Society for Photogrammetry and Remote Sensing Annual Conference, ASPRS 2013*, pp. 653.

Yu, C.-., Wu, K.-. & Wang, C.-. 2011, "A distortion-free data hiding scheme for high dynamic range images", *Displays,* vol. 32, no. 5, pp. 225-236.

Tiant, Q., Duantt, J. & Qiuttt, G. 2012, "GPU-accelerated local tone-mapping for high dynamic range images", *Proceedings - International Conference on Image Processing, ICIP*, pp. 377.